Research Article

Development of Self-Swelling Tablets as a Substitute for Soundless Cracking Demolition Agents

Shuai Xu,[1] Runran Li,[1] Zhangchao Li,[1] Xubo Ji,[1,2] and Fidelis T. Suorineni [3]

[1]*Key Laboratory of Ministry of Education for Safe Mining, Northeastern University, Shenyang, Liaoning, China*
[2]*Shandong Humon Smelting Co. Ltd., Yantai, Shandong, China*
[3]*School of Mining and Geosciences, Nazarbayev University, 53 Kabanbay Batyr Avenue, Nur-Sultan 010000, Kazakhstan*

Correspondence should be addressed to Fidelis T. Suorineni; fsuorineni@gmail.com

The low viscosity of soundless cracking demolition agent (SCDA) slurries makes them difficult to use on rock and concrete breakage in horizontal and up holes, or wet holes. In this paper, self-swelling tablet cartridges are developed by use of additives including adhesive, wetting agent, water absorbent, and activator to SCDA powder through newly developed production technologies. The dosages of adhesive and wetting agent were optimized in the process of powder granulation. Their optimal addition amounts are 3.17% and 11.81%. The self-swelling tablet (SST) experiments and optimization tests show the hardness of SST improved with an increase in pressure and mold filling height. Subsequently, laboratory tests were conducted to determine the influence of the contents of water absorbent and activator on the SST water absorption, reaction temperature, and expansion pressure. The water absorption of SST was found to improve with an increase in water absorbent amount and particle size of the granules. The optimum dosage of the water absorbent is 10%. Based on the laboratory experiments, the optimum amount of additives in the SST is 5% for its best performance. The production of SST cartridges is in a safer and healthier environment compared to SCDA powder cartridges, and its production can be automated to reduce labour cost. Finally, the introduction of SST cartridges expands the scope of application of the SCDA to up holes, horizonal holes, and wet holes.

1. Introduction

Rock breaking is widely used in the fields of mineral resource extraction and underground space development, among which the drill and blast method is the most common approach. The drill and blast production cycle is discrete with time loss in between activities, thereby often resulting in reduced productivity such as the slow tunnelling advance rate. Moreover, noise and dust pollution caused by drilling and blasting are serious environmental and health hazards. With the intensification of environmental issues and search for production efficiency to reduce cost, it is vital to seek other efficient rock-breaking methods.

Soundless cracking demolition agents (SCDAs) are a powdery concrete and rock-breaking material developed in Japan in the 1980s [1]. The main component of static cracking demolition agents is calcium oxide which can react with water and then crystalize and expand. In drill holes and other constrained spaces, the expansion volume of the hydrated SCDA is limited, resulting in the creation of pressure on the hole wall that fractures the concrete or rock mass when the hoop stress [2] exceeds its tensile strength [3–5]. Compared with other concrete and rock breakage methods, the rock fracturing process of SCDAs is characterized by no noise, no vibration, no air pollution, and no fly rocks [6, 7]. SCDA concrete and rock fracturing technology is often applied in such fields as construction demolition and dimension stone quarrying [8, 9]. In recent years, studies on SCDAs have made it possible to extend their applications to oil and gas production [10]. With further research, the development prospects of SCDAs are continuously improving, and their application is extending to other fields such as mining [11].

SCDAs are usually in powder form with a particle size between 20 μm and 100 μm. The expansion of the SCDA in its application is achieved by mixing it with a certain amount of water to form slurry which is then injected into the hole of the medium to be fractured. The expansion pressure produced by the SCDA slurry is closely related to its water content, and therefore, a direct application to water holes cannot be achieved [12, 13] since the water content in the hole can increase the water content of the applied SCDA above the required water content to make it ineffective. However, the distribution of water within the rock mass is extremely complex, and water inrush often occurs in blastholes [14–16]. Consequently, a reduction of the SCDA per unit volume of water leads to a decrease in expansion pressure, which reduces the SCDA capacity to fracture the rock or concrete. Another problem with the use of the SDCA is in its use in upward or horizontal holes for concrete and rock breakage. In up holes and horizonal holes, the SDCA slurry automatically flows out [9, 17, 18] unless the hole is shallow and narrow [19]. Therefore, SCDA slurry can only be used in near horizontal or downward drilled holes [20]. Furthermore, the exothermal reaction of SCDAs with water can result in elevated temperatures to generate water vapor to cause blowout from holes, which can reduce its expansion pressure and/or cause injury to workers and damage equipment. The potential injury to personnel and damage to equipment can result from the gas impact force produced from the blowout and the corrosive alkaline powder discharged [5, 21].

The large specific surface area of SCDA powder makes it easy to contact and react with water in the air to render it inert when used as the expansive agent, and vacuum packaging is widely adopted for SCDAs. However, when the packaging is incomplete or damaged, SCDAs are exposed to water in the atmosphere and react with it, resulting in its effectiveness on use. Additionally, it is on record that CaO exothermal reaction can cause fire when in contact with organic materials such as straw due to the elevated temperatures generated from such reactions [22].

To resolve these issues, manufacturers and researchers have attempted to make SCDA powder into cartridges for packaging and storage [23, 24]. As SCDAs need to absorb water in the process of use, their cartridge external packing materials should have good water permeability. Such cartridge covering materials include a kraft paper and permeable fabric. However, because these packing materials have insufficient rigidity, they are easily damaged by strong air flow during the wrapping of SCDAs with the powder packing machine. Consequently, the preparation of SCDA powder cartridges relies on manual labor that is laborious and time-consuming in a hazardous environment where workers must endure extreme SCDA dust conditions in the packaging process [24]. Besides, workers are challenged in controlling the charge density in the process of preparing the cartridges due to the fine particle size and the free flow of SCDA powder.

The application of SCDA powder cartridges with different densities will have different water absorbing capacities under the same conditions and will result in uneven water-

SCDA ratios. When the water-SCDA ratio is small, the expansion pressure of SCDA slurry is especially small and results in ineffective rock or concrete breakage. On the other hand, high water-SCDA ratios result in the phenomenon of slurry blowout where reactants run off rapidly from the hole, thereby leading to reduced expansion pressure and inefficient fragmentation. In effect, the improvement in the packaging of the SCDA as SCDA powder cartridges is less than satisfactory.

Based on the manufacturing process of effervescent tablets [25], this study investigates packaging SCDA powder in the form of self-swelling granules with the powder granulation technique by adding an adhesive, a wetting agent, a water absorbent, and an activator as excipients to SCDA powder. In the study, the granules are made into the self-swelling tablet (SST) of optimally determined hardness by adjusting the manufacturing process parameters. Laboratory tests are then conducted on the tablets to determine their water absorption and expansion pressure characteristics to evaluate their reaction behaviour with water to evaluate the expansivity of the SST. Finally, the SST is applied to concrete specimens to verify its fracturing effectiveness. While the current experiments did not include rock, it is assumed that the effectiveness of the SST in fracturing concrete can be extended to rock as already demonstrated by Mitri [11].

The SST can be applied to such fields as rock breakage, demolition of concrete structures, and blasthole stemming. The significance of this study is in the expansion of the utilization of SCDAs, extending their fields of application and improving construction and worker safety. Unlike the use of the traditional SCDA powder, the SST can be applied in up holes, horizontal holes, and wet holes.

2. SST Preparation Materials and Methods

2.1. Preparation Materials of the SST

2.1.1. Static Cracking Demolition Agent. The soundless cracking demolition agent (SCDA) is a powder mixture of calcium oxide and trace amounts of silicate, calcium aluminate, boric acid, citric acid, and naphthalene or solid polycarboxylic superplasticizer. The SCDA is the main component of the proposed SST. The volume expansion of the SCDA is due to $Ca(OH)_2$ ettringite crystals, calcium silicate hydrate, and other silicates produced by the hydration of calcium oxide [26–28]. Among these compounds, $Ca(OH)_2$ and calcium silicate hydrate are the main components in the hydration process of the SCDA and are responsible for the early strength increase and expansion pressure generated in the hydration process. Silicate and ettringite enhance the generation of the expansion pressure [29]. The main reaction of the hydration of SCDAs can be expressed as in the following equation:

$$CaO\,(s) + H_2O\,(l) = Ca\,(OH)_2\,(s)\Delta H = \frac{-64.8\,kJ}{mol}. \qquad (1)$$
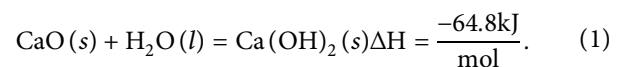
In equation (1) s = solid, l = liquid, and H = heat generated from the exothermal reaction.

2.1.2. Excipients. (1) Poly (1-Vinylpyrrolidone-Co-Vinyl Acetate).

Due to the fine particle size and low cohesion of SCDA powder, adhesive excipients are added to increase the cohesion of SCDAs. Poly (1-vinylpyrrolidone-co-vinyl acetate) (PVP/VA) is a water-soluble and alcohol-soluble polymer resin. PVP/VA has good cohesion, low water absorption, and super solubility. This is because PVP/VA is a linear random organic polymer copolymer from the hybrid reaction of N-vinylpyrrolidone (NVP) and vinyl acetate (VA). PVP/VA is commonly used in the preparation of various powdery and granular materials [30]. Due to the fine particle size effect, good cohesion, low water absorption, super solubility, and high uniformity of granulation, PVP/VA was chosen as the adhesive in the preparation of the SCDA self-swelling tablet (SST).

(2) Anhydrous Ethanol.

PVP/VA alone is not sufficient to provide SCDAs enough cohesion. Thus, the tablet preparation cannot adopt the technology of direct powder compression and hence requires the addition of a wetting agent to further enhance the cohesion of SCDA powder particles.

Anhydrous ethanol is a common organic solvent with high viscosity to enhance SCDA cohesion and can be produced by dissolving PVP/VA. Gibbs free energy of the reaction of anhydrous ethanol, PVP/VA, and CaO is positive and cannot influence the hydration reaction of SCDAs [31]. Moreover, anhydrous ethanol is the best choice to moisturize SCDA powder due to its low toxicity and price. Therefore, the study chose anhydrous ethanol as the moisturizing agent for further enhancement of the SCDA cohesion properties.

(3) Super Absorbent Polymer.

The structure of the proposed SST will be impermeable if it has a high density and strength, as there will be little capillary action to influence its water absorption capacity. Thus, a super absorbent polymer (SAP) should be added to increase its water absorption capacity. The SAP is a hydrolysis product from a copolymer of starch and acrylonitrile, with its main components being starch and acrylate. The SAP can generate electrolysis after contacting water. On contacting water SAP dissociates into positive and negatively charged cations and anions, respectively, both of which have strong hydrophilicity that makes the SAP a high water-retaining material. The molecular structure of the SAP is a reticular molecular chain with 3-D cross-linking bridging, resulting in higher concentration of the internal ions to result in osmotic pressure to quickly absorb water many times higher than its own. Due to the advantages of SAP rapid absorption and retention of water in substantial amounts, it is selected as the SST's water absorbent to increase its water absorption capacity.

(4) Activator.

The addition of enhanced viscosity excipients to SCDAs results in the decrease of their specific surface areas and reduces the reaction rate between water and the CaO to decrease the reaction rate of SST tablets. Hence, activators should be added to SCDAs to increase their reaction rate. The principle of aluminum-water system activation is that the mixture of aluminum powder and alkaline material reacts with water to generate substantial amounts of heat. The activator should be characterized by a fast heating rate, super heating efficiency, and a long persistent period with temperature up to 260°C [32]. Since the reaction environment is alkaline, the subsequent reactions of SCDAs are almost unaffected before or after the reaction of the activator. Therefore, adopting adding an activator of the aluminum-water system to the SST can improve its reaction rate.

2.2. Self-Swelling Tablet Preparation Methods

2.2.1. Process.

Due to the poor flowability of SCDA powder, it is necessary to first increase the size of the particles by granulation and then convert the granules into the tablets. In the granulating process SCDAs, cohesion, the wetting agent, and other excipients are uniformly mixed to form a soft consistent moldable material after vibration mixing. Next, by the method of forced extrusion, the moldable materials are transformed into granules through controlled-size sieve gauges. The indicator for forming quality of granules is the particle yield ratio defined in equation (2). If the particle yield ratio is less than 20%, the amount of wetting cohesive agents in the SST is adjusted.

$$\beta = \frac{m_2}{m_1} \, x100\%, \qquad (2)$$

where β is the particle yield, m_1 is the weight of the raw material, and m_2 is the weight of the granules.

After the granules' preparation, the granules with a uniform particle size are mixed with the water absorbent and the mixture is placed in the tablet pressing mold to obtain the SST with certain hardness under a particular pressure. If the hardness of the tablets is less than 300 N (according to the vibration test result), it is necessary to adjust the manufacturing parameters in the tableting process, such as pressure, filling height, and particle size until the required hardness is obtained. The process of converting the SCDA powder to a self-swelling tablet is shown in Figure 1.

2.2.2. Equipment

(1) Granulating Equipment.

The YBZ-60 Swing granulator (Figure 2) was selected for the granulation. The granulator cylinder diameter is 60 mm with a motor capacity of 0.55 kW, and the number of swings is forty-six times/min for a granule production capacity of 20–30 kg/h.

(2) Tableting Equipment.

The YP-30T hydraulic powder tablet press (Figure 3) was used for making the SST. The press pressure range of the machine is from zero kN to 300 kN. The pressure can be controlled from an analogue pressure gauge with a measurement accuracy of 0.1 kN with a head diameter of 110 mm and pressure measurement accuracy of 0.1 MPa/min. In underground mines, drill hole diameters in medium length blastholes are usually from
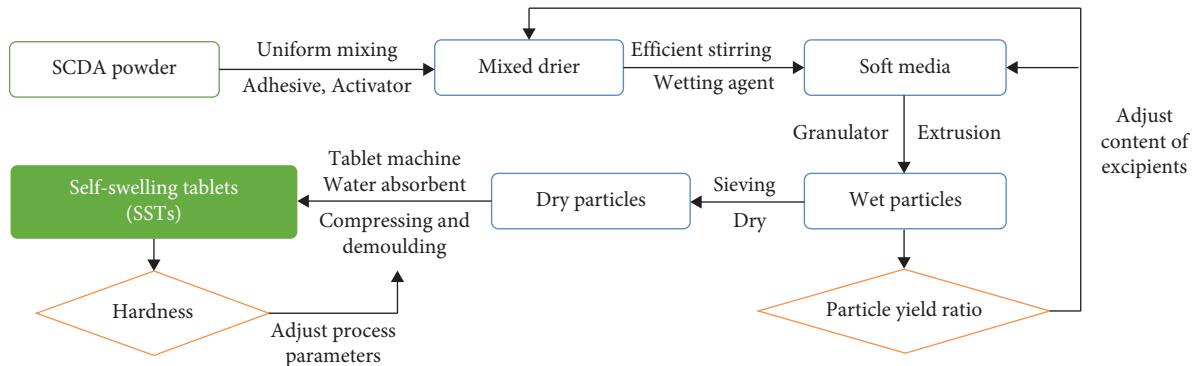
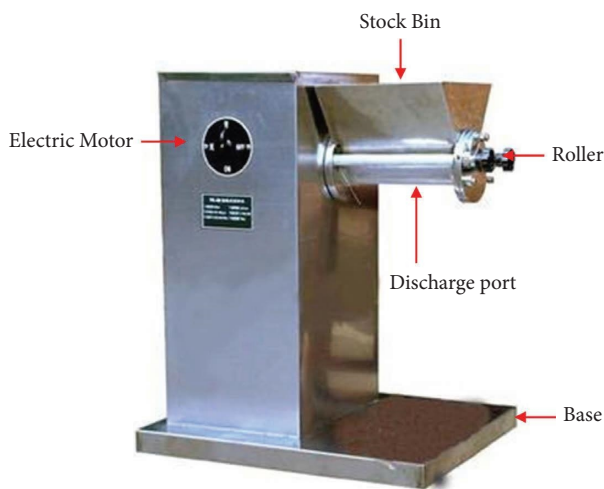FIGURE 1: The self-swelling tablet (SST) preparation flowchart.
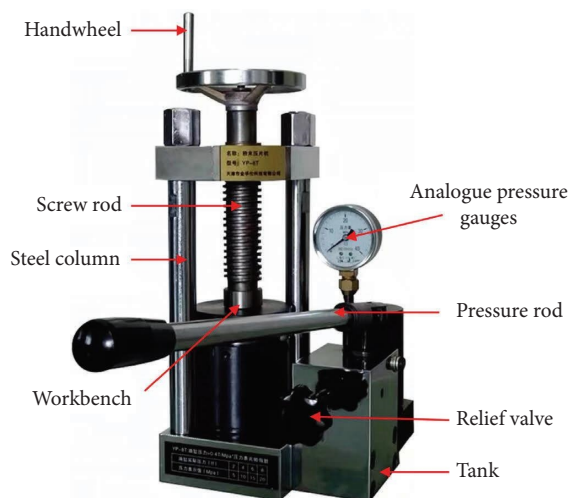

FIGURE 2: The YBZ-60 swing granulator.

FIGURE 3: YP-30T hydraulic powder tablet press.

60 mm to 120 mm. Thus, a stainless-steel base mold with an inner diameter of 80 mm is selected for the tableting preparation. The mold precision is 0.5 mm, its filling height is up to 6 cm, and the height of tablets range between 2 cm and 4 cm.

(3) Hardness Test Equipment.

The hardness test equipment is a Humboldt HM-5030 loading-test machine shown in Figure 4. The machine pressure sensor precision is 0.01 N, the displacement measurement accuracy is 0.001 mm, the maximum loading capacity is fifty kN, and the loading rate is fixed at 1 N/s.

3. Preparation of SST Experiments

3.1. Particle Yield Ratio Optimization in the SCDA Power Granulation Process

3.1.1. Analysis of Influencing Factors on the Particle Yield Ratio. As shown in Figure 1, the SST preparation includes two phases of powder granulation and tablet formation. In the granulation process, the amount of adhesive and wetting agents affects the cohesiveness of the resulting soft medium. When the soft medium cohesiveness is too high, it is easy for granulators to produce strips when extruding the soft medium, and the strips will hinder the formation of granules. On the other hand, it is difficult for granulators to produce granules when the soft medium adhesiveness (bonding) is too low. Therefore, appropriate dosages of adhesive and wetting agents are vital for increasing the particle yield ratio.

3.1.2. Experimental Design for Particle Yield Ratio Optimization. The particle yield ratio is determined by the amounts of adhesive and wetting agents used, and therefore, the experimental design involves only the two factors. Reasonable levels of the ratio of anhydrous ethanol to SCDAs are 10%, 12%, and 14%, and of PVP/VA to SCDAs are 2%, 3%, and 4% [33]. Granules are produced according to the process flow chart shown previously in Figure 1. The resulting granules are sieved through numbers 15 and 35 in sequence. The resultant granules, which are in the particle size range of 15–35 mesh, are weighed, and the results are input into equation (2) for m_1 and m_2 to determine the particle yield ratio (β). The experimental design and results are shown in Table 1.

3.1.3. Test Results of Particle Yield Ratio Optimization. The particle yield ratio optimization test results are given in Figure 5. When the amount of anhydrous ethanol is
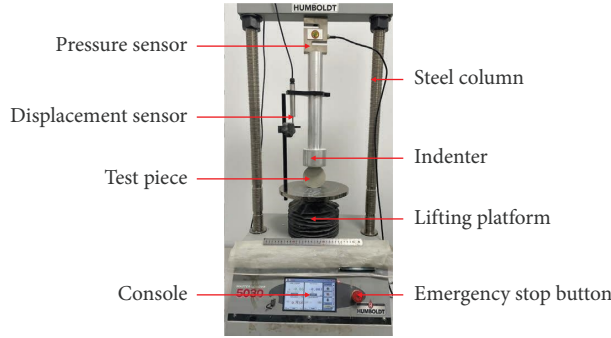
FIGURE 4: The Humboldt HM-5030 loading test machine.

TABLE 1: Three level comprehensive experimental design of anhydrous ethanol and PVP/VA.

Case	01#	02#	03#	04#	05#	06#	07#	08#	09#
Anhydrous ethanol (%)	10	10	10	12	12	12	14	14	14
PVP/VA (%)	2	3	4	2	3	4	2	3	4
Particle yield ratio (%)	12.80	13.00	10.77	27.50	30.19	29.20	3.53	5.16	1.79
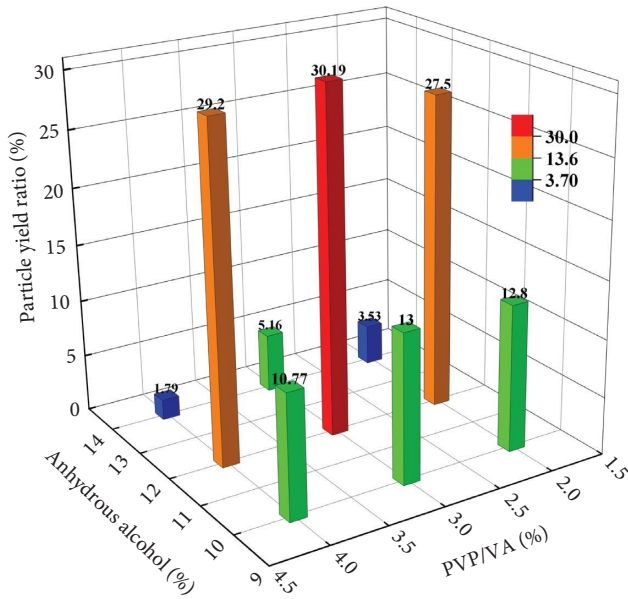
FIGURE 5: Effect of anhydrous alcohol and PVP/VA on the particle yield ratio.

TABLE 2: Goodness of fit of the particle yield ratio.

Source	Sequential p value	Adjusted R-squared	Predicted R-squared	
Linear	0.6980	−0.1827	−0.8338	
2FI	0.8481	−0.4078	−2.3563	
Quadratic	<0.0001	0.9962	0.9857	Suggested
Cubic	0.6677	0.9949	0.8845	Aliased

particle yield ratio. First, the experimental results of the particle yield ratio are examined through tests of goodness of fit to select its polynomial form. The results are shown in Table 2. Quadratic models provide the best goodness of fit, and the difference in value between the adjusted R^2 and predicted R^2 is less than 0.2, implying that the quadratic model is the acceptable model.

The experimental results in Figure 5 are iterated through the least square method to get the quadratic model shown in equation (3).

$$r = -69.19 + 122.53a - 1.37p + 0.68ap - 5.28a^2 - 1.04p^2, \tag{3}$$

where $r = \beta$ is the particle yield ratio, a is the anhydrous ethanol content, and p is the PVP/VA amount.

Next, variance analysis was used to determine the rationality of the above model, as shown in Table 3. The F value of the model is 421.42 which is larger than an F value of 9.02 in the F-distribution Table 3, where $\alpha = 0.05$ and the degree of freedom (df) is (5, 3), indicating that the model is significant. A p value of 0.002 is far less than 5%, which indicates the effective significance of the whole model. The signal to noise ratio (SNR) of the model is 50.01, indicating that it is far higher than four and implying that the model can be used to navigate the design space.

The contrasts between actual particle and predicted particle yield ratios are given in Figure 6. The scatter in experimental results is uniformly distributed about the

constant, the particle yield ratio increases first and then decreases with the rise of PVP/VA, indicating that an optimal content of PVP/VA exists in that interval. When PVP/VA amount is constant, the particle yield ratio also increases first and then decreases with the raise in anhydrous ethanol amount. However, changes of the latter are greater than changes of the former, implying that the effects of anhydrous ethanol content on the particle yield ratio are greater than the impacts of PVP/VA at their respective factor levels.

3.1.4. Analysis and Optimization of the Particle Yield Ratio. According to the experimental results shown in Table 1, the response surface method [34] is adopted to optimize the

TABLE 3: Variance and significance of the factors governing the particle yield ratio.

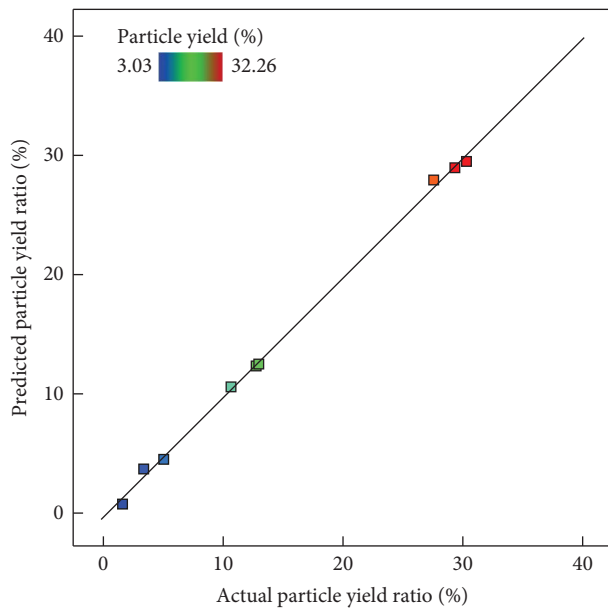| Source	Sum of squares	df	Mean square	F value	p value Prob > F	
Model	1016.68	5	203.34	421.42	0.0002	Significant
a-anhydrous ethanol	113.45	1	113.45	235.12	0.0006	
p-PVP/VA	1.54	1	1.54	3.19	0.1720	
ap	7.29	1	7.29	15.11	0.0302	
a^2	892.25	1	892.25	1849.21	<0.0001	
p^2	2.15	1	2.15	4.45	0.1253	
Residual	1.45	3	0.4825			
Cor total	1018.12	8				

FIGURE 6: Comparison between actual and predicted values of the particle yield ratio.

straight-line $y = x$, indicating that the fitting model and experimental values are in good agreement. Thus, it is feasible to adopt the model for optimizing and analyzing the particle yield of the self-swelling granules.

Finally, a contour chart and D-surface graph are plotted with anhydrous alcohol and PVP/VA as independent variables and particle yield as a dependent variable, as shown in Figure 7. According to the contour chart and the D surface graph, the particle yield changes with the variation of anhydrous alcohol, implying that the particle yield is affected by the amount of anhydrous alcohol. According to the optimization results from the above model, the optimal proportion of anhydrous alcohol and PVP/VA is shown in Table 4.

Validation experiments were conducted based on the optimal proportion of anhydrous alcohol and PVP/VA given in Table 4 and the processes described below. The components of the anhydrous alcohol and PVA/VA were weighed with electronic scales as 500 g of SCDAs, 59.05 g of anhydrous alcohol, and 15.85 g of PVP/VA. Five steps were taken in the sample preparation process, which are as follows: mixing, granulating, drying, sieving, and weighing

in sequence. The average particle yield determined was 30.63%, which is remarkably close to the result from the optimizing model, and the relative error between the experimental results and the predicted ones is less than 5%, reflecting high reliability of the particle yield ratio through the optimizing model in the granule preparation of SCDAs. According to the optimization and validation results, when the amount of anhydrous alcohol is 3.17%, the particle yield is optimized.

3.2. SST Hardness Parameter Optimization

3.2.1. Analysis of Influencing Factors on Tablet Hardness. The SST hardness is the force which is needed to break the tablet under only radial pressure. Since in the process of tablet preparation only three factors, namely, pressure, particle size, and filling height can be controlled, the tablet hardness is related to these factors. Pressure is the force that the tablet machine's indenter applies on the sample. The particle size is the average particle size of all the granules, it is controlled by the screen mesh size, and filling height is the height of the material loaded into the tablet mold. Single factor and factorial experiments were designed to confirm whether the three factors and their interactions are significant influence factors on the tablet hardness [35].

(1) Single Factor Experiment on Tablet Hardness.
A single factor experiment is an experimental method in which only one factor is changed, while holding the other factors constant. Single factor experiments were used to analyze the significant effects of individual factors in their respective level intervals. According to the allowable parameters of the equipment, pressure was from 50 kN to 150 kN, filling height was from 2 cm to 6 cm, and the particle size was from sieves of mesh sizes 15 to 35. The experimental design is shown in Table 5.

The experiments were conducted in accordance with Figure 1, and each experiment was repeated three times. The average of each set of three experimental results was taken and summarized in Figure 8. Figure 8 shows that the tablet hardness increases with the advance in pressure and filling height, but it increases and then decreases with the increase in the particle size.

The flowability of self-swelling granules is poor when the particle size is small. Flowability determines compressibility and influences the tablet hardness. With the increase in the particle size, particle flowability improves and hardness
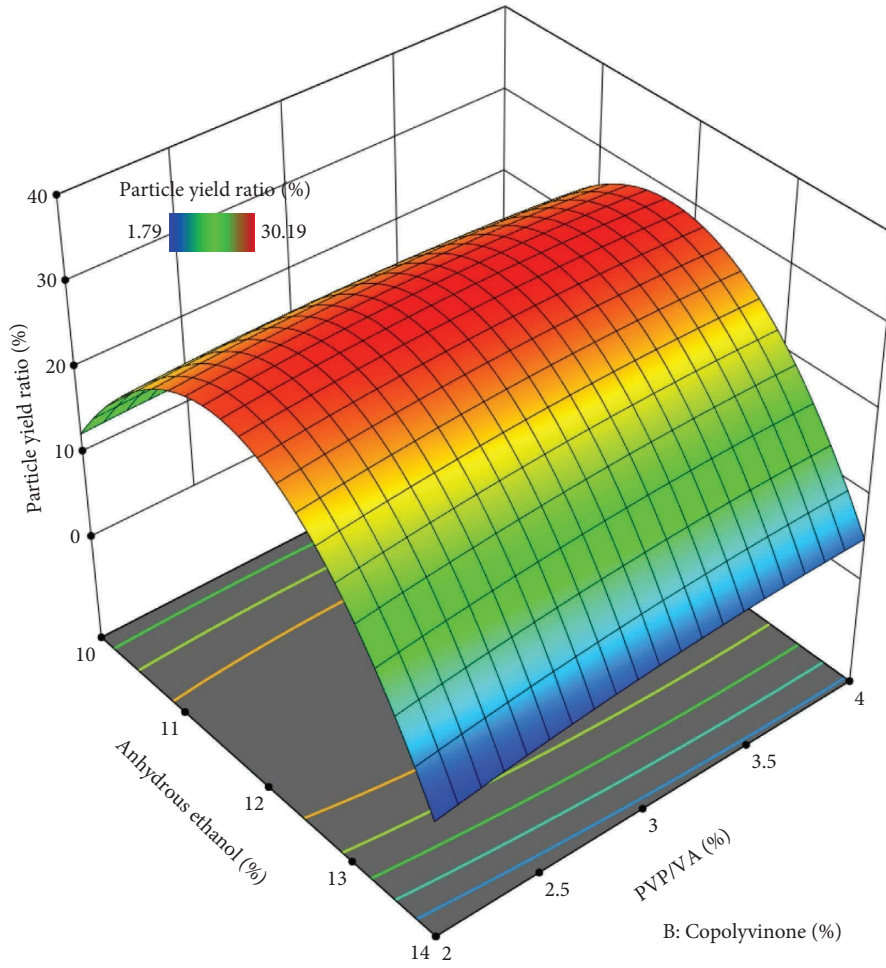
FIGURE 7: The response surface model of the particle yield ratio.

TABLE 4: The optimization scheme of the particle yield ratio.

Anhydrous ethanol (%)	PVP/VA (%)	Particle yield ratio theoretical value (%)	Confidence (%)	Evaluate
11.81	3.17	30.63	99.6	Suggested

TABLE 5: Single factor experimental design of SST hardness.

Case	01#	02#	03#	04#	05#	06#	07#	08#	09#
Pressure (kN)	50	100	150	100	100	100	100	100	100
Particle size (mesh)	25	25	25	15	25	35	25	25	25
Packing height (cm)	6	6	6	6	6	6	2	4	6

increases. However, when the particle size is too large, the internal porosity of the tablets decreases and results in easy damage of the tablets by compaction under external forces, which results in the decrease in tablet hardness.

According to the experimental results, the equations relating each of the three factors (pressure (p), filling height (h), and particle size (d)) to the tablet hardness are given by equations (4)–(6), respectively.

$$S = -183.05 + 6.56p - 0.01p^2, \tag{4}$$

$$S = -270.25 + 177.67h - 10.24h^2, \tag{5}$$

$$S = -1320.2 + 122.6d - 2.11d^2, \tag{6}$$

where S is the tablet hardness, p is the applied pressure, h is the mold filling height, and d is the particle size.

Equations (4) to (6) were investigated by analysis of variance methods, and the results are shown in Table 6. F values of the three models are all larger than the F value of 19 in the F-distribution table, where $\alpha = 0.05$ and degree of freedom is (2, 2), indicating that the model is significant. When the p value is smaller than 0.05%, it indicates that the significance of the model is valid. The values of p, h, d, p_2, h_2, d_2, F, and p involved in the model satisfied the significance
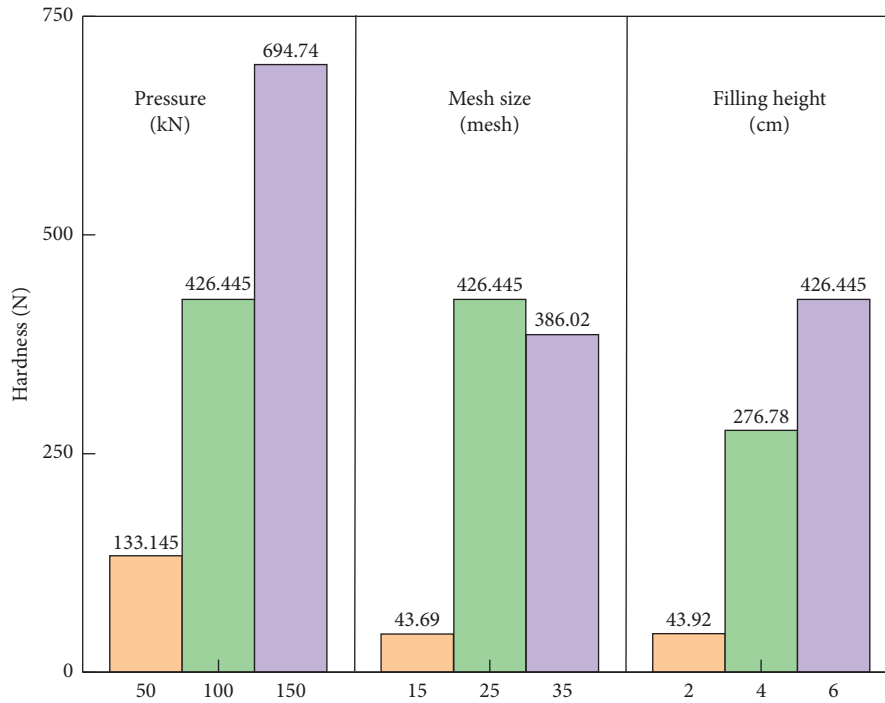
FIGURE 8: Summary of single factor SST hardness test results.

TABLE 6: Variance and significance of three influencing factors on SST hardness.

Source	Sum of squares	df	Mean square	F value	p value Prob > F	
p-model	$3.155E + 005$	2	$1.578E + 005$	$4.059E + 005$	<0.0001	Significant
p-pressure	$3.154E + 005$	1	$3.154E + 005$	$8.116E + 005$	<0.0001	
p^2	111.34	1	111.34	286.51	0.0035	
Pure error	0.78	2	0.39			
Cor total	$3.155E + 005$	4				
h-model	$1.477E + 005$	2	73834.02	23169.98	<0.0001	Significant
h-packing height	$1.463E + 005$	1	$1.463E + 005$	45918.61	<0.0001	
h^2	1342.67	1	1342.67	421.35	0.0024	
Pure error	6.37	2	3.19			
Cor total	$1.477E + 005$	4				
d-model	$1.528E + 005$	2	76383.91	22388.81	<0.0001	Significant
d-particle size	$1.172E + 005$	1	$1.172E + 005$	34349.39	<0.0001	
d^2	35577.99	1	35577.99	10428.23	<0.0001	
Pure error	6.82	2	3.41			
Cor total	$1.528E + 005$	4				

requirement. The results show that all the three factors have significant influence on the tablet hardness.

(2) Factorial Experiment on Tablet Hardness.

The factorial experiment on the three factors with each at two levels was adopted to confirm whether pressure, particle size, filling height, and their combinations are significant factors on the SST hardness. The factor groups are formed by the combination of factors and levels to fully reflect the interaction among them (Table 7).

The experiment was conducted according to the steps shown in Figure 1. Each group of the experiments was repeated three times, and the average value was taken. The results are summarized in Figure 9. Figure 9 shows that

TABLE 7: Three factor two-level factorial experiment of SST hardness.

Case	01#	02#	03#	04#	05#	06#	07#	08#
Pressure (kN)	50	150	50	150	150	50	50	150
Packing height (cm)	6	2	6	2	6	2	2	6
Particle size (mesh)	15	15	35	35	15	35	15	35

particle hardness increases at various levels with the increase in pressure, particle size, and filling height, which is consistent with the trend observed in the single factor experiments. In addition, when the pressure is 50 kN and the particle size is 15 mesh size, the filling height increased from
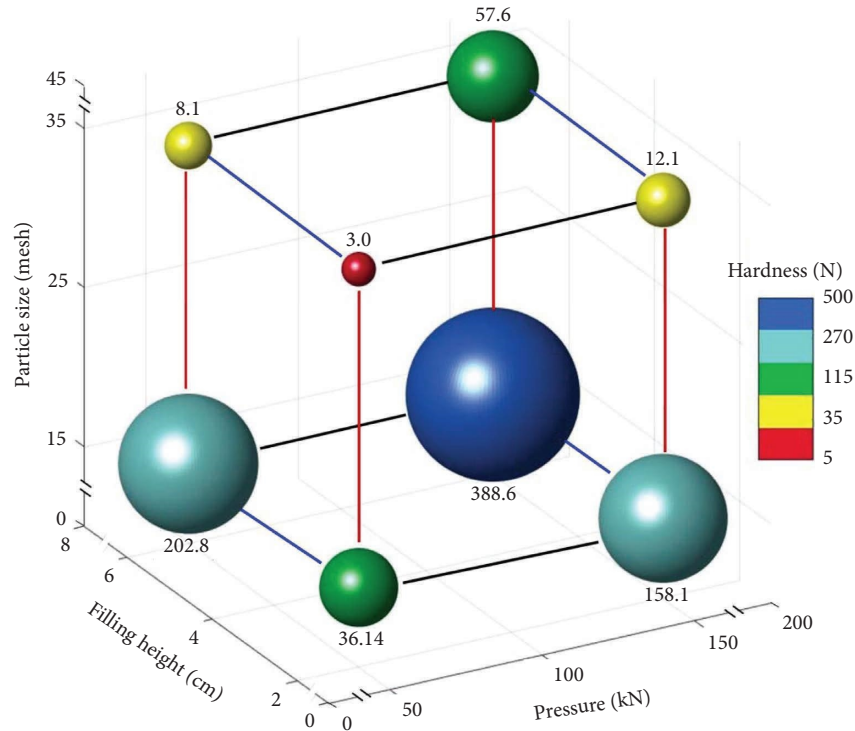
FIGURE 9: Summary of three factors and two-level SST hardness test results (numbers on spheres represent the tablet hardness for that condition).

2 cm to 6 cm and the tablet hardness increased from 36.14 N to 202.2 N, which is an increase of 166.66 N. However, other conditions remaining unchanged, when the particle size is 35 mesh, the tablet hardness increased from 3 N to 8.1 N, which is an increase of 5.1 N, indicating a significant decrease. Therefore, the effects of any factor on the tablet hardness can change with the other levels of factors, implying that there may be non-negligible interactions among the factors.

According to the factorial experiment test results on the three factors, each at two levels, a mathematical model was obtained with actual values of factors as independent variables (equation (7)).

$$S = -195.2 + 1.95p + 69.12h + 6.08d - 0.06pd - 2.17dh, \quad (7)$$

where S is the hardness, p is the pressure, h is the filling height, and d is the particle size.

The variance analyses are shown in Table 8. The F value in Table 8 is 312.88 which is larger than the F value of 234.0 in the F-distribution table, where $\alpha = 0.05$ and the degree of freedom is (6, 1), implying that the model is significant. Because of the noise, the probability of error is less than 4.32%. Hence, the probability of less than 5% indicates the effective significance of the whole model. For p, h, d, ph, pd, and hd in the model, P values are all less than 0.05, implying that the model items are valid, and the three factors and their interaction items are important influencing factors on the tablet hardness.

3.2.2. Experimental Design for Tablet Hardness Optimization.
The significant factors affecting the self-swelling tablet hardness are pressure, particle size, and mold filling height.

The levels of these factors for pressure are 50 kN, 100 kN, and 150 kN; for particle size are 15 mesh, 25 mesh, and 35 mesh; and for mold filling height are 2 cm, 4 cm, and 6 cm, respectively. The self-swelling tablets were prepared according to the steps in Figure 1 for these factor levels, and the tablet hardness tests were conducted using a loading machine shown in Figure 4. The experimental scheme and results are shown in Table 9. In Table 9, the experiments numbered 1, 13, 16, and 18 are repeated experiments.

(1) Analysis of Results on Tablet Hardness Optimization Tests.

The test results of tablet hardness optimization are plotted in Figure 10. The size of a ball represents the hardness of the tablet. The larger the ball, the higher the hardness of the tablet. The X, Y, and Z axes in Figure 10 represent the pressure, particle size, and filling height, respectively. The results show that the hardness of tablets increased with an increase in the three factors. The data are better explained with a response surface method plot in the next section.

(2) Response Surface Plot.

According to the experimental results shown in Table 9, the response surface method was applied to better explain the results. First, the hardness test results were evaluated by model fitting, and a polynomial form was found as the best fit. The results are shown in Table 10. The P value of the sequence model and its simulation error are less than 0.05, and the coefficient of determination (R^2) is close to one. The difference between the coefficient of determination and the adjusted R^2 is not more than 0.2. Hence, the predicted value of the quadratic polynomial is the optimal fit to the data.

TABLE 8: Variance and significance of three factors and the two-level factorial experiment on SST hardness.

Source	Sum of squares	df	Mean square	F value	p value Prob > F	
Model	1.281E + 005	6	21341.77	312.88	0.0432	Significant
p-pressure	16775.62	1	16775.2	245.94	0.0405	
h-packing height	25049.93	1	25049.3	367.24	0.0332	
d-particle size	62099.93	1	62099.93	910.41	0.0211	
ph	11354.08	1	11354.08	189.85	0.0406	
pd	9756.35	1	9756.35	153.71	0.0495	
hd	15014.71	1	15014.71	220.12	0.0428	
Residual	68.21	1	68.21			
Cor total	1.28E + 005	7				

TABLE 9: Central composite experimental results on SST hardness.

Case	Pressure (kN)	Particle size (mesh)	Packing height (cm)	Actual value
01#	100	25	4	194.12
02#	50	35	2	13.01
03#	50	15	2	16.14
04#	100	15	4	102.83
05#	50	25	4	127.82
06#	100	25	6	325.74
07#	50	35	6	38.10
08#	150	35	6	137.59
09#	50	15	6	202.84
10#	150	25	4	307.91
11#	150	15	2	158.14
12#	150	15	6	388.56
13#	100	25	4	198.54
14#	150	35	2	32.14
15#	100	35	4	76.37
16#	100	25	4	195.06
17#	100	25	2	133.17
18#	100	25	4	195.40

According to the above experimental results, the least square method was used to iterate the experimental results in Table 9, and the relationship between the predicted value of the tablet hardness as a function of pressure, particle size, and filling height is as shown in equation (8).

$$S = -738.55 + 0.84p + 63.97d + 15.73h - 0.05pd$$
$$+ 0.16ph - 1.79dh + 0.01p^2 - 1.15d^2 + 6.32h^2, \quad (8)$$

where S is the tablet hardness, p is the applied pressure, h is the filling height, and d is the particle size.

Variance analysis was used to determine the rationality of equation (8), and the results are shown in Table 11. The F value of the model is 19.95, which is higher than the F value of 3.39 with $\alpha = 0.05$ and degree of freedom (9, 8) in the F distribution table, implying that the model is significant. The P value of 0.001 is far less than 5%, indicating that the significance of the whole model is acceptable. The F value of 450 means that the model is significant, and the probability of error is less than 0.01% and far less than 5%. It is determined that the model has a signal to noise ratio of 16.55, which is much higher than four, confirming that the model can be used to navigate the design space.

Figure 11 shows the comparison between the experimental and predicted values of the hardness of the self-swelling tablets. The scattered points are evenly distributed on the $y = x$ line, indicating that the fitting model is in good agreement with the experimental results. Thus, it is feasible to use this model to predict the hardness of the self-swelling tablets.

Finally, the factors governing the tablet hardness were ranked in order of their importance in influencing the tablet hardness. By considering each pair of two factors of pressure, particle size, and mold filling height as independent variables and the tablet hardness as the dependent variable, the experimental results are presented in as a 3D surface model as shown in Figure 12. Figure 12 shows that for a given pressure in a certain range of the particle size, the tablet hardness is more affected by the particle size; and for a given pressure in a certain range of filling height, the hardness is more affected by the particle size; and for a certain range of the particle size and filling height, the hardness is more affected by the applied pressure.

In summary, the significance of the influencing factors on particle hardness is in the order of filling height > particle size > pressure. According to the model in equation (8), the maximum tablet hardness can be obtained within the
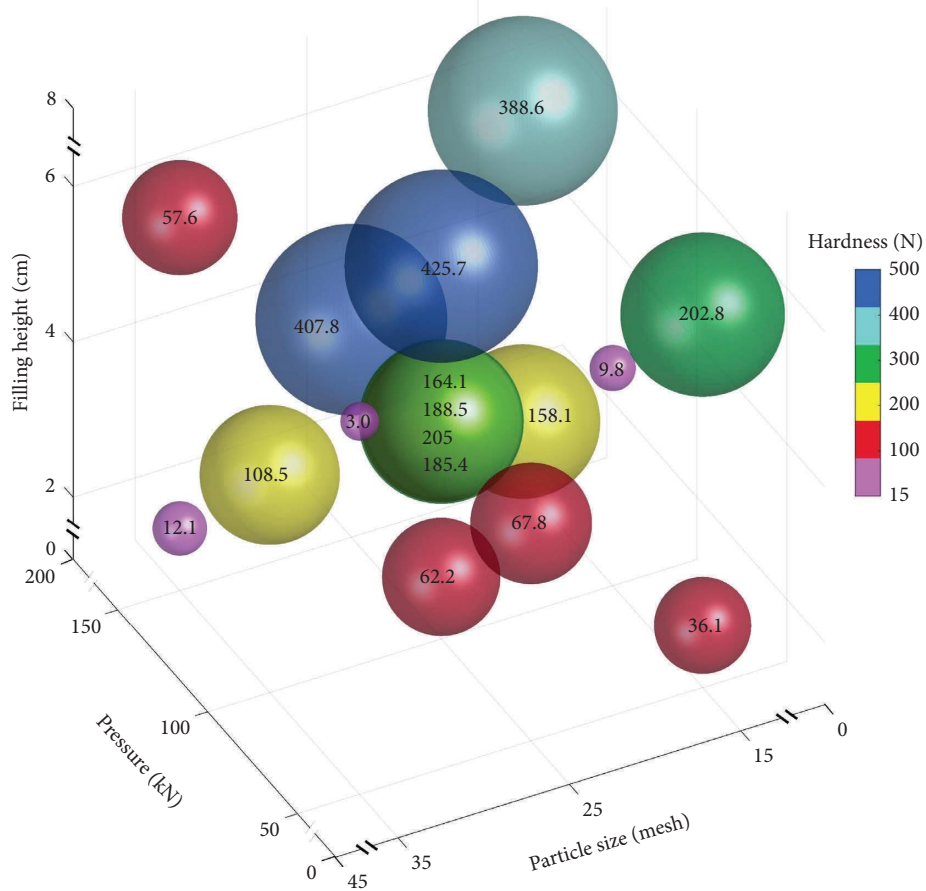
FIGURE 10: Results of SST hardness optimization tests (numbers on spheres represent the tablet hardness for that condition).

TABLE 10: Goodness of fit of SST hardness tests.

Source	Sequential p value	Lack of fit p value	R^2	Adjusted R^2	
Linear	0.0016	<0.0001	0.6512	0.5765	
2FI	0.3263	<0.0001	0.7420	0.6013	
Quadratic	0.0017	0.0002	0.9573	0.9093	Suggested
Cubic	0.0017	0.0058	0.9990	0.9957	Aliased

TABLE 11: Variance and significance of the factors affecting SST hardness.

| Source	Sum of squares	df	Mean square	F-value	p value	
Model	$1.862E + 05$	9	20690.52	19.95	0.0001	Significant
p	39241.45	1	39241.45	37.83	0.0003	
d	32638.37	1	32638.37	31.47	0.0005	
h	54794.05	1	54794.05	52.83	<0.0001	
pd	5465.35	1	5465.35	5.27	0.0508	
ph	1924.48	1	1924.48	1.86	0.2103	
dh	10266.01	1	10266.01	9.90	0.0137	
p^2	507.61	1	507.61	0.4894	0.5040	
d^2	35573.02	1	35573.02	34.29	0.0004	
h^2	1731.27	1	1731.27	1.67	0.2325	
Residual	8298.17	8	1037.27			
Lack of fit	8287.14	5	1657.43	450.55	0.0002	Significant
Pure error	11.04	3	3.68			
Cor total	$1.945E + 05$	17				
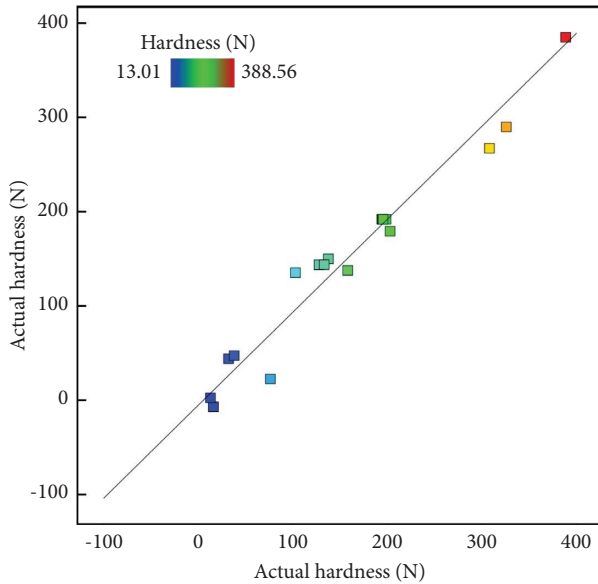
Figure 11: Comparison between experimental and predicted SST hardness values.

selected factor level range when the pressure is fixed at 120 kN. This is because the tablets become too dense under the applied pressure, which affects the subsequent tablet water absorption capacity. The optimum tablet hardness is obtained for a particle size range of 15–35 mesh size, filling height range of 0–6 cm, and a pressure of 120 kN as shown in Table 12.

To verify the reliability of the optimization results, five identical pieces of the SST were made, with the pressure set as 120 kN, the particle size set at 20 mesh size, and the filling height placed at 6 mm. The hardness test was conducted on the five samples. The results show that the average hardness was 363.19 N, which is the best value for all the five tablets, and the relative error between the experimental results and the predicted ones is less than 5%, confirming that the model is accurate and the experimental results are reliable.

4. Experiment for Evaluation of the Hydration Reaction Rate of the Self-Swelling Tablets

The self-swelling tablets developed in the research have high density and hardness, but their hydration properties such as the water absorption rate that governs its reaction rate and expansion pressure have not been ascertained. By adding a water absorbent and an activator in the SST preparation process, the hydration reaction of the tablets can be optimized so that the tablets can gain better expansion for rock and concrete fracturing.

4.1. Experimental Scheme for Investigating the Hydration Reaction of the Self-Swelling Tablets

4.1.1. Super Absorbent Polymer (SAP) Content Test. Water absorption of the SST refers to the percentage of the mass of absorbed water in its saturated condition. The water

absorption of the SST determines its expansion pressure as a minimum amount of water is required for its complete hydration reaction.

The sample used for testing was a cylindrical cartridge with a diameter of 50 mm and a height of 100 mm. This cartridge consisted of four SSTs, each with a diameter of 50 mm and a height of 25 mm. To prevent crumbling of the SST during the water absorption test, the samples were completely wrapped with a kraft paper with four 2 mm × 2 mm openings evenly punched on the side with a knife. The openings were then sealed with a semipermeable material. This was to prevent the slurry containing SCDA powder from flowing out from the opening. The tablets were completely soaked in water at an ambient temperature of 20°C. They were then removed, drained, and weighed using an electronic balance every 30 s until the moisture content remained constant on subsequent weighing. This process generally lasted for about 10 minutes. When the moisture content of the tablets was no longer changing (the SST was considered to have reached water absorption saturation), the process was terminated, and the water absorption rate was calculated. Each group of experiments was repeated three times, and the average was taken. The test scheme is shown in Table 13.

4.1.2. Activator Content Test. The quick reaction of an activator with water generates a large amount of heat, which increases the ambient temperature and speeds up the hydration reaction of the SST. Zero to thirty percent of the activator and 10% of 20 mesh size absorbent granules were added to the water and tablets, respectively. The contents of other excipients remained unchanged. The ratio of SST component raw materials is shown in Table 14.

After soaking in water for 10 minutes at 20°C, the SST mass was determined, and it was allowed to react freely in a hollow aluminum ingot. A PT100 temperature sensor was used to measure the temperature change during the reaction process, and the upper end surface method (UESM) [24] was employed to determine its expansion pressure.

In the UESM procedure, the SST is prepared and immersed in water according to the procedure in Section 4.1.1 and then placed into the UESM device. The UESM device consists of an outer cylinder upper end surface and an inner pipe. The outer pipe upper end surface is used to attach strain gauges to measure the expansivity of the SST in the inner pipe. After connecting strain gauges to the outer cylinder upper surface, the tangential and radial strains on the UESM device during SST expansion can be obtained and used to calculate the expansivity of the SST.

4.2. SST Hydration Reaction Results

4.2.1. Influence of SAP Content on Water Absorption and the Rate of Water Absorption of Tablets. The hydration reaction test results are shown in Figure 13. When the dosage of the SAP is 5% and the particle size is 20 and 30 mesh, the water absorption of the self-swelling tablets is 31% and 29.3%, respectively, after 10 minutes. Studies have shown that, when
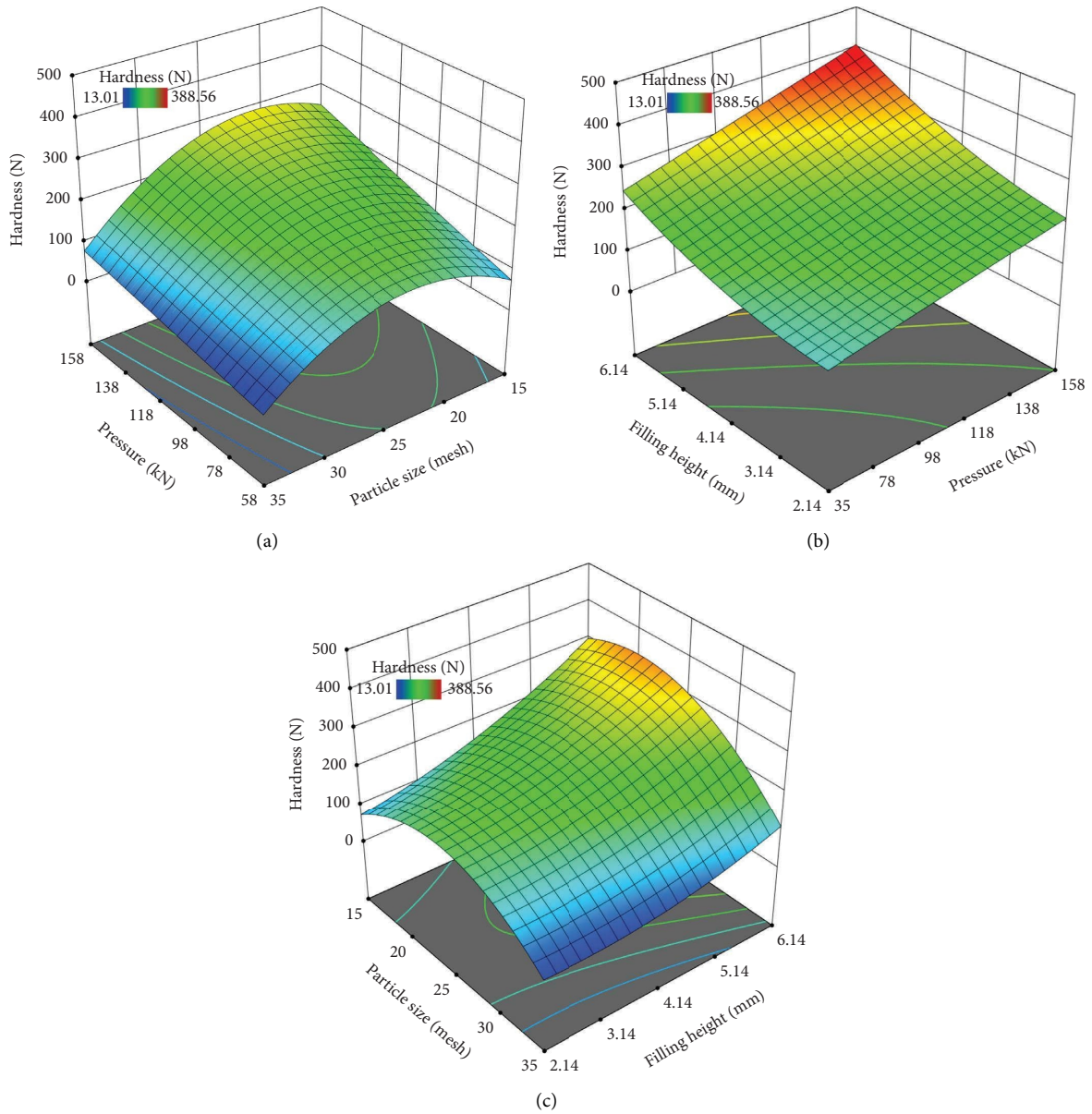
Figure 12: The response surface model of SST hardness: (a) variation of SST hardness with pressure and particle size, (b) variation of SST hardness with mold filling height and applied pressure, and (c) variation of SST hardness with particle size and mold filling height.

Table 12: The SST hardness optimization scheme.

Pressure (kN)	Particle size (mesh)	Packing height (cm)	Hardness theoretical value (N)	Confidence (%)	Evaluate
120	20	6.00	361.97	99.8	Suggested

Table 13: Experimental design of water absorption of the SST.

Case	01#	02#	03#	04#	05#	06#
Ratio (%)	0	5	10	5	5	5
Grain diameter (mesh)	20	20	20	10	20	30

TABLE 14: Experimental design of activator content.

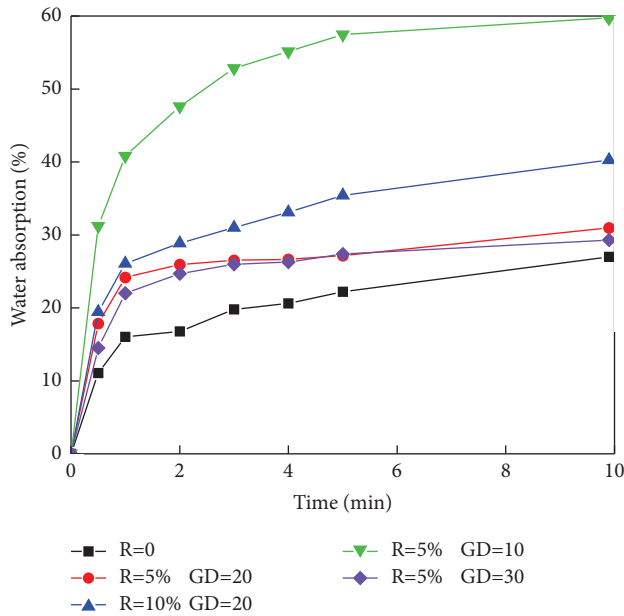| Case	SST quality (g)	Activator (g)	Ratio (%)
01#	240	0	0
02#	240	12	5
03#	240	24	10
04#	240	36	15
05#	240	48	20
06#	240	60	25
07#	240	72	30

FIGURE 13: Effect of the water absorbent on SST water absorption with time.
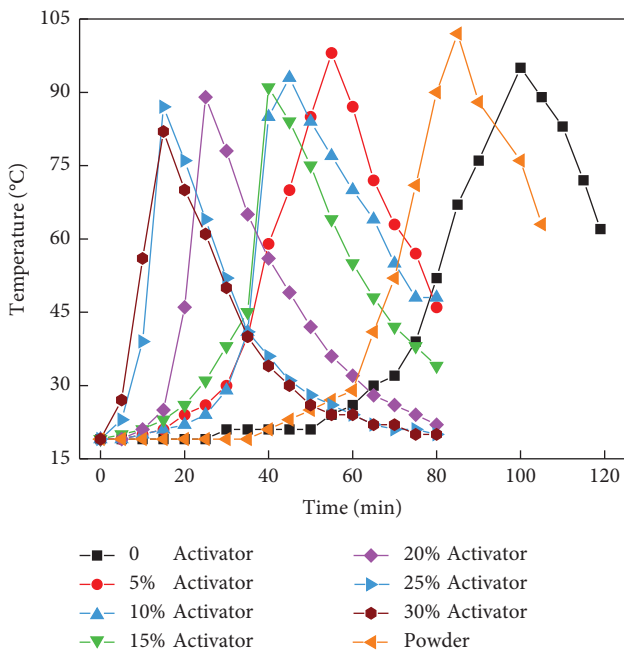

FIGURE 14: Effect of activator amount on SST reaction temperature with time.

the water absorption exceeds 50%, the expansion pressure of SCDAs is reduced [36, 37]. Therefore, on the premise of increasing the water absorption, the optimal SAP particle size in the tablets is 20 mesh and the optimal dosage is 10%.

It can be seen from Figure 13 that the larger the SAP particle size, the higher the water absorption ability of the SST. Large SAP granules result in high number of voids even after pressing, and therefore, free water is more easily absorbed due to capillarity. When the SAP particle gets smaller and is more densely packed with SCDAs in a tablet, free water cannot fully percolate into the tablets and be absorbed due to limited capillarity. When the SAP particle size is 20 mesh and the dosage is 0, 5%, and 10%, the water absorption of the tablets is 27%, 31%, and 40.2% respectively, after 10 minutes, implying that the dosage of the SAP has a greater influence on the water absorption than the particle size. Hence, the water absorption ability of the SST increases with boost in SAP dosage.

4.2.2. Influence of Activator Dosage on the Tablet Hydration Reaction Rate of the SST. The test results of the reaction rate are shown in Figure 14. The SCDA powder begins to react when taken out after soaking in water for 40 minutes, and the reaction temperature peaks at 102°C after 85 minutes.

With the addition of an adhesive and a wetting agent with no activator, the SST reaction starts after 50 minutes, with the reaction temperature peaking at 95°C after 100 minutes. This indicates that the addition of an adhesive and a wetting agent has a significant inhibition effect on the reaction rate of SCDAs. When 5 to 15% activator is added, the hydration reaction is immediate on soaking in water, and the reaction peak temperature is reached after 40–60 minutes. Compared with the SST without the activator, the time taken to reach the peak temperature is 50% less, indicating that the activator does react first and plays a role in driving the SCDA reaction. However, when the dosage of the activator increases to 20%, the reaction rate of the SST increases significantly, reaching the peak temperature of 90°C in 25 minutes. This peak temperature is the same as that of tablets with low dosage of the activator. When the dosage of the activator is higher than 20%, the reaction rate increases slightly with no significant change in peak temperature, indicating that the reaction ability of SCDAs is fully achieved when the dosage of the activator is 20% or higher.

4.2.3. Influence of Activator Dosage on Water Absorption and Expansion Pressure of the SST. The water absorption and expansion pressure of the SST changed with increased activator dosage, as shown in Figure 15. With the increase in the dosage of the activator, the water absorption of the tablets changed slightly with the activator dosage increase of 1.4%, from 35.9% to 37.3% after 10 minutes, while the expansion pressure decreased by 6.8 MPa, from 30.7 MPa to 23.9 MPa. The water absorption of the tablet does not change significantly with the addition of the activator, but the expansion pressure increased first and then decreased significantly with the increase in activator dosage. Based on
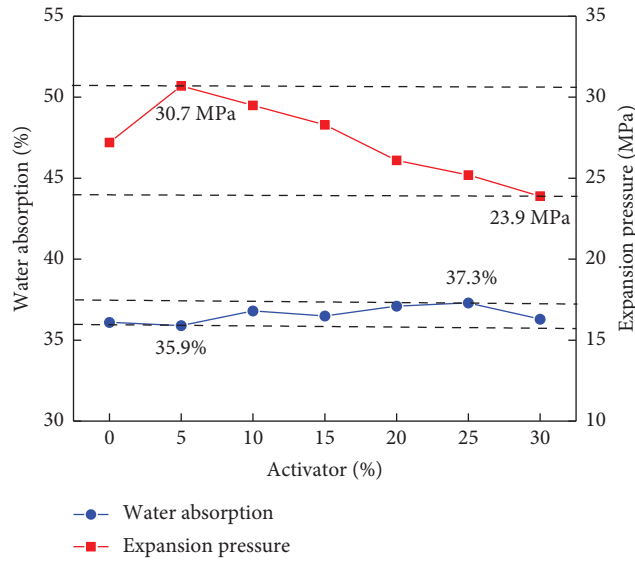
FIGURE 15: Effect of activator content on SST expansion pressure and water absorption.

TABLE 15: Test data on the 30 MPa uniaxial compressive strength concrete block.

Case	UCS (MPa)	Elastic modulus (GPa)	Poisson's ratio
01#	30.03	29.64	0.28
02#	31.24	30.11	0.30
03#	39.88	30.74	0.24
Average value	33.72	30.16	0.27

Figure 15, the optimum amount of activator dosage is determined as 5%.

As shown in Figure 15, the optimum water absorption of the SST is 35–38%, higher than the 20–30% of SCDA powder alone whose expansion pressure can reach 20–90 MPa [38]. The expansion pressure of the SST is slightly less than the SCDA. This is because although the water absorption of the SST is high due to the addition of the SAP, water is difficult to percolate into the tablets due to its lower permeability.

5. Evaluation of Fracturing Capacity of the SST

To verify that the SST has good expansion capacity to fracture concrete and rock, a test of concrete block was used. Blocks of concrete specimens, 30 cm in length, 30 cm in width, and 25 cm in height, with a compressive strength of 30 MPa, were made. A circular hole with a diameter of 82 mm and a length of 25 cm was made in the center of the block along its height. The same raw materials used in molding the blocks were used to conduct standard uniaxial compression tests. The mechanical properties of the concrete blocks were obtained through the uniaxial compression tests and shown in Table 15.

Eight tablets with a height of 3 cm were packed in a kraft paper to be prepared as cartridges according to the steps introduced in Section 3. The cartridges were soaked in 20°C water at room temperature for 10 minutes and were then placed in the hole in the center of the concrete block. The SST expansion effect on the concrete block was monitored with a digital speckle correlation method (DICMS) as shown in Figure 16.

The concrete block fracturing process was captured in real time as shown in Figures 17 and 18. Figure 17 was taken after 18 minutes ($t = 0.3$ hours) following the SST hydration reaction and shows obvious stress concentration on the surface of the concrete block around the hole because of the SST expansion. The maximum principal strain at stress concentration location was about 0.26-0.27% as measured with the upper end surface method (UESM) [24]. As the hydration reaction time increased, the stress concentration area increased. After 0.6 hours of the tablet hydration reaction time, the strain on the concrete block increased to about 0.33–0.36%. At this time, microcracks were developed in the lower part of the stress concentration area of the block. With continuous increase in the tablet expansion, the cracks completely developed along the central axis of the block after the tablet hydration reaction was 1.3 hours. The block was completely split into two parts after the tablet hydration reaction time of 1.5 hours. The average crack aperture was measured to be 22.2 mm with a maximum crack width of 31.1 mm.

The SST expansion concrete block fracturing test results show that the SST produced can fracture concrete on hydration and expansion. Considering the mechanical properties of the block, the SST developed can be used to fracture concrete structures and rock with less health risks compared to the use of the SCDA powder. In addition, the nature of the
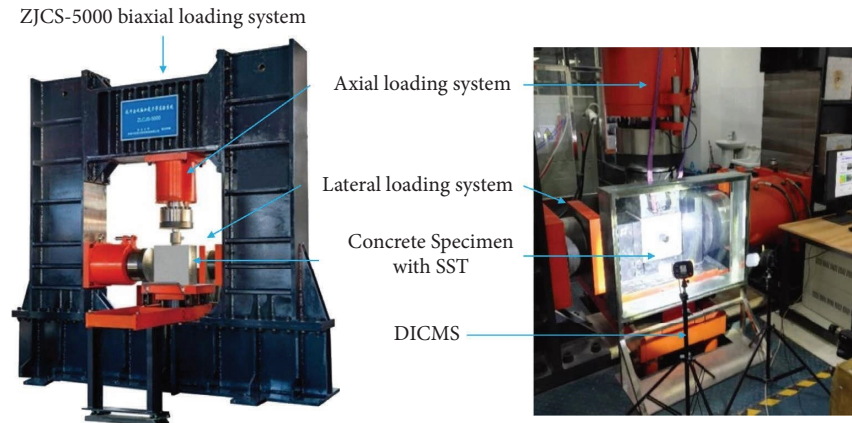
FIGURE 16: The SST fracturing capacity test on the 30 MPa uniaxial compressive strength concrete block.

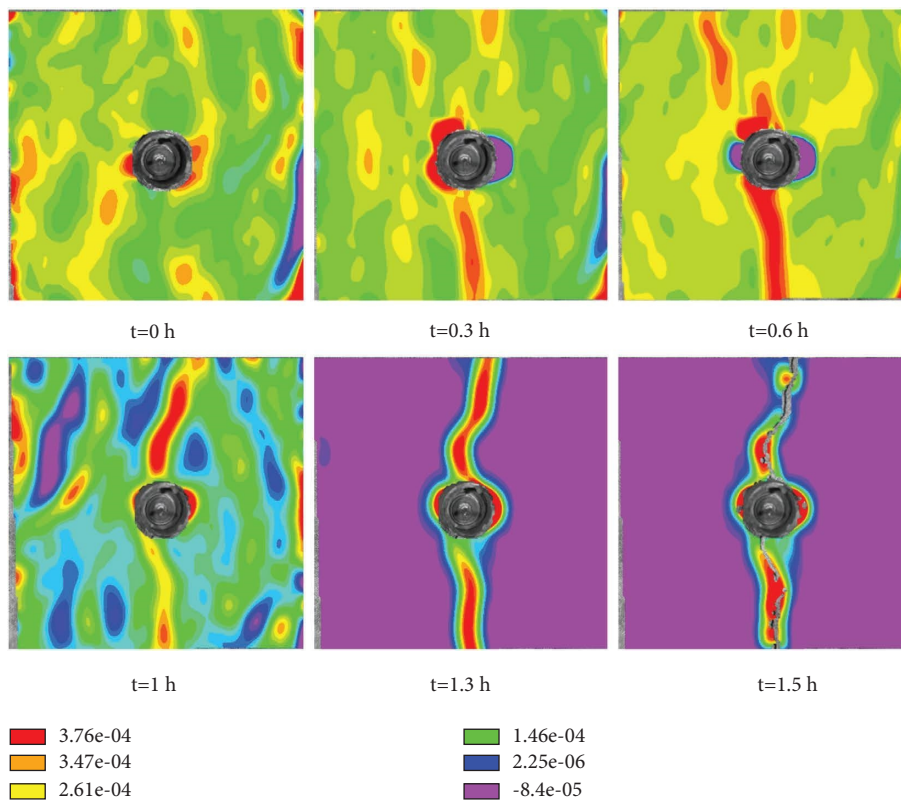|		
3.76e-04		1.46e-04
3.47e-04		2.25e-06
2.61e-04		-8.4e-05

FIGURE 17: Monitoring results of SST expansion fracturing of the concrete block with time using a DICMS.

SST makes it suitable for the fracturing of rocks in water filled holes, up holes, and horizontal holes, where the traditional SCDA may only be applicable with difficulty.

6. Analysis and Discussion of Results

6.1. SST Water Absorption. The average water absorption rate of the SST with different particle sizes at a SAP content of 5% is shown in Figure 18. The horizontal axis in the figure labeled as "Code" with values of −2, 1, 0, 1, and 2 represent particle sizes of 50 mesh, 40 mesh, 30 mesh, 20

mesh, and 10 mesh, respectively, or SAP contents of 0%, 5%, 10%, 15%, and 20%, respectively. The figure shows that the water absorption rate increases with gain in the SAP particle size (red curve).

When the particle size of the water absorbent is 20 mesh, the −2, −1, 0, 1, and 2 codes in the figure represent the five SAP contents of 0%, 5%, 10%, 15%, and 20%, respectively. Due to the difference in strength of the SAP and the self-swelling granules, with the increase in the SAP particle size, the porosity of the tablets increases, and the tablets' water
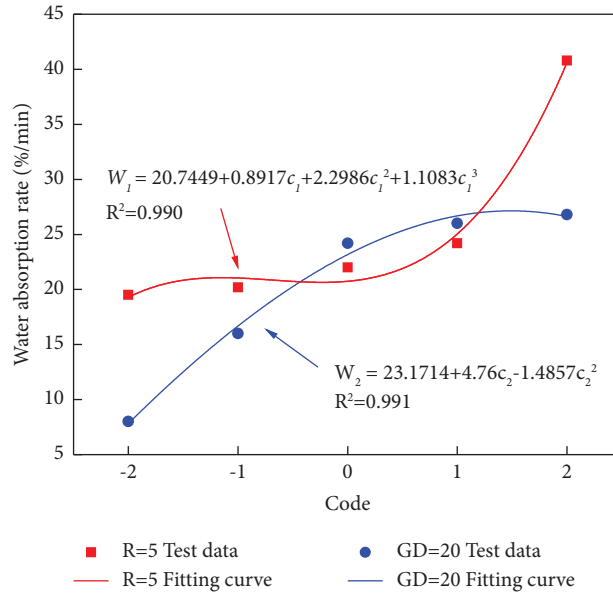
$$W_1 = 20.7449+0.8917c_1+2.2986c_1^2+1.1083c_1^3$$
$$R^2=0.990$$

$$W_2 = 23.1714+4.76c_2-1.4857c_2^2$$
$$R^2=0.991$$

FIGURE 18: The fitting curve of the water absorption rate of the SST with different particle sizes and amounts of the water absorbent.
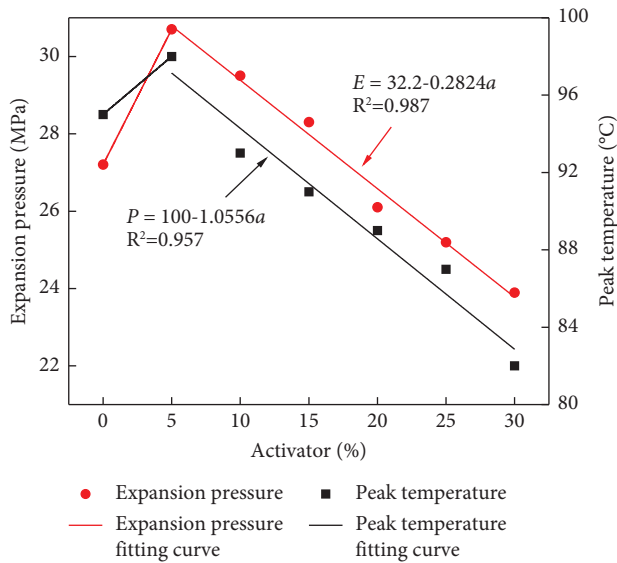

$$E = 32.2-0.2824a$$
$$R^2=0.987$$

$$P = 100-1.0556a$$
$$R^2=0.957$$

FIGURE 19: SST peak temperature and expansion pressure with an increase in activator content.
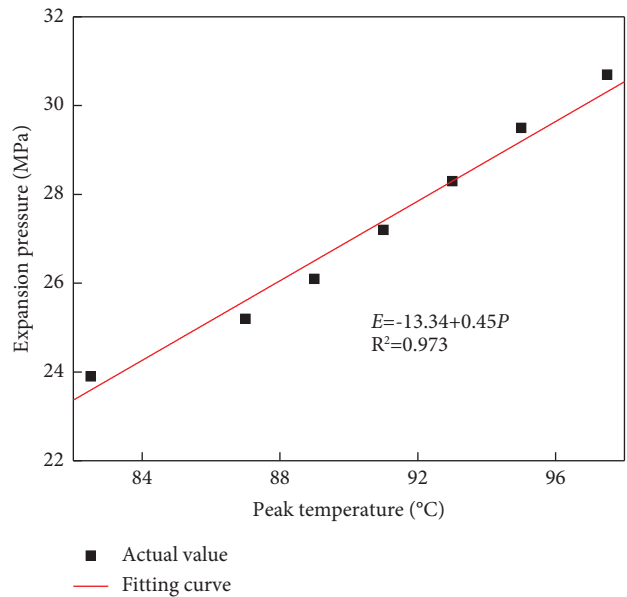

$$E=-13.34+0.45P$$
$$R^2=0.973$$

FIGURE 20: Relationship between peak temperature and swelling pressure of different SSTs (numbers are percentage amounts of activator content).

absorption rate rises rapidly, resulting in a higher water absorption rate.

On the other hand, the water absorption rate of the SST increases and then remains constant after code 1 (equivalent to 15% SAP content) with further boost in SAP content. The first half of the curve shows that the water absorption rate rapidly increases with SAP content. The implication is that there is a water absorption saturation value of the tablets, above which the water

absorption rate of the tablet has negligible effect with change in SAP content.

TABLE 16: Recommended components of the SST for optimum performance.

Factor	SCDA (%)	Anhydrous ethanol (%)	PVP/VA (%)	SAP (%)	Activator (%)
Content (amount)	100	11.81	3.17	5–10	10

6.2. Analysis of the Expansion Characteristics of the SST. Figures 14 and 15 represent the peak temperature and expansion pressure of the SST, respectively. Figure 14 shows that the peak temperature of the SST increases first and then decreases with further increase in activator content. Similarly, in Figure 15, the expansion increases with activator content up to peak and decreases. The reason for the increase in expansion pressure and peak temperature with activator content is that the addition of an activator causes some previously unreacted SCDAs to participate in the reaction, promoting the reaction and making it closer to a complete reaction. The expansion pressure and peak temperature decrease from the peak is due to the decrease in the proportion of SCDAs in the tablet as the content of the activator increases in the same volume. The lost amount of the SCDA is greater than the amount of SCDAs that the activator requires to enhance the reaction. This observation is more evident in Figure 19.

It is determined that the activator content in the tablets is 5% or more, and the peak temperature and water absorption decrease by 17°C and 1.4% for an expansion pressure difference of 6.8 MPa, respectively, on average. As shown in Figure 19, with the change in activator amounts, the trend of the temperature and expansion pressure curves of the tablets are similar. According to the temperature and expansion pressure at the same activator content, the peak temperature—expansion pressure scatter diagram and the fitting model of the scatter distributions are shown in Figure 20. When the reaction peak temperature of the tablet increases from 82°C to 98°C, the expansion pressure increases from 23.9 MPa to 30.7 MPa. This is because the expansion pressure and peak temperature of the tablet depend on the amount of activator involved in the reaction. When the activator decreases, the peak temperature and expansion pressure increase correspondingly and vice versa. This linear relationship provides a new calculation method for the prediction of expansion pressure for given reaction temperatures and vice versa.

7. Conclusion

Static cracking demolition agents (SCDAs) are well known in the demolition of concrete structures and in the production of dimension stones. Recently, their application has been extended to rock breakage in mining. The low viscosity of SCDA slurries from a mixture of SCDA powder and water for placement in demolition holes makes them difficult to use on rock and concrete breakage in horizontal and up holes or wet holes. The SCDA powder packaging is also a challenge; it is environmentally unfriendly with associated health risks.

In this paper, self-swelling tablet (SST) cartridges are developed by use of additives of an adhesive, a wetting agent, a water absorbent and an activator to the SCDA powder through newly developed production technologies.

Experiments were designed and used to determine the optimum amounts of expedients in the SST for its optimum performance in concrete and rock breakage. Table 16 summarizes the additives needed and their optimum amounts for an effective SST in concrete and rock breakage.

Hardness is the key index for measuring the successful production of self-swelling tablets. The factors affecting the hardness of self-swelling tablets primarily include pressure, particle size, and mold filling height. The importance of these three factors is in the order of mold filling height, particle size, and pressure. The hardness increases with growth in filling height and pressure, and it increases first and then decreases with the increase in the particle size.

The performance of the developed self-swelling tablets in fracturing concrete and rock was demonstrated in the laboratory using concrete blocks. The tests proved that the SST has good concrete fracturing ability like the traditional SCDA powder when mixed with water. As concrete can be likened to rock, we postulate that the SST could equally fracture rock given the proper design of the SST holes.

Compared with SCDA powder, the SST is more convenient for transportation and storage. The production of the SST is in a safer environment, provides better health conditions to workers, and improves labor productivity. In addition, compared with SCDA cartridges, the SST preparation process is automated and reduces labor cost. The SST also extends the application of the SCDA to use in up holes, horizontal holes, and wet holes.

Data Availability

All data generated in the research are included within the article.

Conflicts of Interest

The authors declare that there are no conflicts of interest.

Acknowledgments

References

[1] Y. Kasai, "Static expansive demolition agent for rock and concrete," *Concrete Journal*, vol. 20, no. 10, pp. 8–17, 1982.

[2] W. Fairbairn, "On steam boilers and the causes of their explosion," *Journal of the Franklin Institute*, vol. 52, no. 2, pp. 128–138, 1851.

[3] Y. Kasai, "The Second International RILEM Symposium on demolition and reuse of concrete and masonry," *Materials and Structures*, vol. 22, no. 4, pp. 312–319, 1989.

[4] S. Chatterji and J. Jeffery, "The volume expansion of hardened cement paste due to the presence of 'dead-burnt' CaO," *Magazine of Concrete Research*, vol. 18, no. 55, pp. 65–68, 1966.

[5] D. Swanson and J. Labuz, "Behavior of a calcium oxide-based expansive cement," *Concrete Science and Engineering*, vol. 1, no. 3, pp. 166–172, 1999.

[6] D. F. Laefer, N. Ambrozevitch-Cooper, M. Huynh, J. Midgette, S. Ceribasi, and J. Wortman, "Expansive fracture agent behaviour for concrete cracking," *Magazine of Concrete Research*, vol. 62, no. 6, pp. 443–452, 2010.

[7] R. V. S. De Silva, R. Pathegama Gamage, and M. Anne Perera, "An alternative to conventional rock fragmentation methods using SCDA: a review," *Energies*, vol. 9, no. 11, p. 958, 2016.

[8] A. S. Natanzi and D. F. Laefer, "Using chemicals as demolition agents near historic structures," in *Proceedings of the 9th International Conference on Structural Analysis of Historical Constructions*, pp. 14–17, Mexico City, Mexico, October 2014.

[9] A. S. Natanzi, D. F. Laefer, and L. Connolly, "Cold and moderate ambient temperatures effects on expansive pressure development in soundless chemical demolition agents," *Construction and Building Materials*, vol. 110, pp. 117–127, 2016.

[10] T. Guo, S. Zhang, H. Ge, and Z. Qu, "A novel "soundless cracking agent fracturing" for shale gas reservoir stimulation," *International Journal of Environment and Sustainable Development*, vol. 6, no. 9, pp. 681–687, 2015.

[11] H. Mitri, "Underground mining without explosives – a mine safety paradigm shift," in *Proceedings of the ISMSSE 2021 Symposium Program*, Katowice, Poland, November 2021.

[12] T. Harada, T. Idemitsu, A. Watanabe, and S. Takayama, "The design method for the demolition of concrete with expansive demolition agents," *Fracture of Concrete and Rock*, Springer, Berlin, Germany, 1989.

[13] J. A. Gambatese, "Controlled concrete demolition using expansive cracking agents," *Journal of Construction Engineering and Management*, vol. 129, no. 1, pp. 98–104, 2003.

[14] D. Ma, H. Duan, and J. Zhang, "Solid grain migration on hydraulic properties of fault rocks in underground mining tunnel: radial seepage experiments and verification of permeability prediction," *Tunnelling and Underground Space Technology*, vol. 126, Article ID 104525, 2022.

[15] D. Ma, H. Y. Duan, J. X. Zhang, X. W. Liu, and Z. H. Li, "Numerical simulation of water–silt inrush hazard of fault rock: a three-phase flow model," *Rock Mechanics and Rock Engineering*, vol. 55, no. 8, pp. 5163–5182, 2022.

[16] D. Ma, H. Y. Duan, J. X. Zhang, and H. B. Bai, "A state-of-the-art review on rock seepage mechanism of water inrush disaster in coal mines," *International Journal of Coal Science and Technology*, vol. 9, no. 1, pp. 50–28, 2022.

[17] W. Nocuń-Wczelik, A. Stok, and Z. Konik, "Heat evolution in hydrating expansive cement systems," *Journal of Thermal Analysis and Calorimetry*, vol. 101, no. 2, pp. 527–532, 2010.

[18] S. Nagataki and H. Gomi, "Expansive admixtures (mainly ettringite)," *Cement and Concrete Composites*, vol. 20, no. 2-3, pp. 163–170, 1998.

[19] A. S. Natanzi, D. F. Laefer, and S. I. Zolanvari, "Selective demolition of masonry unit walls with a soundless chemical demolition agent," *Construction and Building Materials*, vol. 248, Article ID 118635, 2020.

[20] W. Tang, C. Zhai, J. Z. Xu, Y. Sun, Y. Z. Cong, and Y. F. Zheng, "The influence of borehole arrangement of soundless cracking demolition agents (SCDAs) on weakening the hard rock," *International Journal of Mining Science and Technology*, vol. 31, no. 2, pp. 197–207, 2021.

[21] C. Li, S. F. He, W. T. Hou, and D. Ma, "Experimental study on expansion and cracking properties of static cracking agents in different assembly states," *International Journal of Mining Science and Technology*, vol. 32, no. 6, pp. 1259–1272, 2022.

[22] I. Tatner, "Calcium oxide and its exothermic reactions," 2017, https://www.hawkins.biz/insights/insight/calcium-oxide-and-its-exothermic-reactions.

[23] T. Kasama, T. Saito, and M. Wada, "Hydration-expansive crushing cartridge," US Patent, Alexandria, VA, USA, US4378997A, 1983.

[24] S. Xu, P. Y. Hou, R. R. Li, and F. T. Suorineni, "An improved outer pipe method for expansive pressure measurement of static cracking agents," *International Journal of Mining Science and Technology*, vol. 32, no. 1, pp. 27–39, 2022.

[25] S. Jacob, A. Shirwaikar, and A. Nair, "Preparation and evaluation of fast-disintegrating effervescent tablets of glibenclamide," *Drug Development and Industrial Pharmacy*, vol. 35, no. 3, pp. 321–328, 2009.

[26] T. Harada, K. Soeda, T. Idemitsu, and A. Watanabe, "Characteristics of expansive pressure of an expansive demolition agent and the development of new pressure transducers," *Doboku Gakkai Ronbunshu*, vol. 1993, pp. 91–100, 1993.

[27] V. S. Ramachandran, P. J. Sereda, and R. Feldman, "Mechanism of hydration of calcium oxide," *Nature*, vol. 201, no. 4916, pp. 288-289, 1964.

[28] S. Chatterji, "Mechanism of expansion of concrete due to the presence of dead-burnt CaO and MgO," *Cement and Concrete Research*, vol. 25, no. 1, pp. 51–56, 1995.

[29] V. De Silva, P. G. Ranjith, M. S. A. Perera, B. Wu, and T. D. Rathnaweera, "Investigation of the mechanical, microstructural and mineralogical morphology of soundless cracking demolition agents during the hydration process," *Materials Characterization*, vol. 130, pp. 9–24, 2017.

[30] R. C. Rowe, P. Sheskey, and M. Quinn, *Handbook of Pharmaceutical Excipients*, Libros Digitales-Pharmaceutical Press, London, UK, 2009.

[31] S. Glasstone, *Textbook of Physical Chemistry*, D. Van Nostrand Co, New York, NY, USA, 1951.

[32] S. Zhang, Y. Liu, and R. Zhong, "Magnesium-water type self-heating material composition," Chinese Patent, Beijing, China, 101475793B, 2011.

[33] Y. Lin, F. C. Qin, L. Zhang, and J. Y. Wu, "Study on preparation technology and dissolution determination of Xin Lv Ning dispersible tablets," *Journal of Chinese Medicinal Materials*, vol. 36, no. 10, pp. 1706–1708, 2013.

[34] L. Vera Candioti, M. M. De Zan, M. S. Cámara, and H. C. Goicoechea, "Experimental design and multiple response optimization. Using the desirability function in analytical methods development," *Talanta*, vol. 124, pp. 123–138, 2014.

[35] X. Li, Y. Liu, and J. K. Yang, "Optimization of Novo435 lipase catalyzed diglyceride ideas production by response surface methodology," *Chinese Journal of Bioprocess Engineering*, vol. 7, no. 5, pp. 13–18, 2009.

[36] J. Hinze and A. Nelson, "Enhancing performance of soundless chemical demolition agents," *Journal of Construction Engineering and Management*, vol. 122, no. 2, pp. 193–195, 1996.

[37] K. Soeda and T. Harada, "The mechanics of expansive pressure generation using expansive demolition agent," *Doboku Gakkai Ronbunshu*, vol. 1993, pp. 89–96, 1993.

[38] S. Xu, P. Y. Hou, R. R. Li, and M. Cai, "An experimental study on the mechanical properties and expansion characteristics of a novel self-swelling cartridge for rock breakage," *Rock Mechanics and Rock Engineering*, vol. 54, no. 2, pp. 819–832, 2021.